International Journal of Pressure Vessels and Piping 201 (2023) 104863

Contents lists available at ScienceDirect

International Journal of Pressure Vessels and Piping

journal homepage: www.elsevier.com/locate/ijpvp

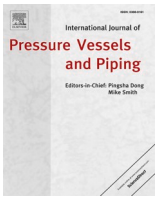

Damage evolution detection in a pipeline segment under bending by means of acoustic emission

Franziska Baensch *, Wolfram Baer, Peter Wossidlo, Abdel Karim Habib

BAM Federal Institute for Materials Research and Testing, Unter Den Eichen 87, 12205, Berlin, Germany

ARTICLE INFO

Keywords:
Acoustic emission
Frequency domain
Potential drop
Cracks

ABSTRACT

A steel pipeline segment of 2.5 m length was subjected to quasi-static four-point bending load in three steps for studying the initial cracking and damage accumulation based on the Acoustic Emission (AE) technique and by the direct current potential drop (DCPD) technique. For the latter, a new post-test analysis method was established. AE is found more sensitive to crack initiation than DCPD. Formation of mesoscopic and macroscopic cracks as well as their closure and the resulting friction generate weighted peak frequencies below 400 kHz, whereas microscopic cracking produces AE with broad band spectra identifiable by weighted peak frequencies above 400 kHz. Critical states alike the maximum load level and the leak opening were accompanied by peak amplitudes above 85 dB_{AE}. This rather fundamental study provides a data base for possibly developing advanced strategies of detection and alarm systems based on acoustic monitoring of pipelines, or at least, steel structures.

1. Introduction

Pipelines are transporting goods, which are becoming more and more very valuable. Consequently, this infrastructure is becoming an additional importance. The service lifetime of steel pipelines might be up to 50 years, whereby the safety and performance of the piping systems must frequently be guaranteed over long distances and multiple branches. Thinking of the large delivery volumes, even a small leak can lead to high costs and severe environmental pollution. Thus, catastrophic incidents are most frequently caused by third party manipulations, e.g. by excavators, agricultural or forestry equipment [1]. However, material composition and manufacture quality, installation as well as environmental conditions influence the durability of the pipeline. Generally, fine-grained steels with low strength but excellent toughness are used for steel piping, because, in case of leak formation, these materials rather generate stable crack growth than unstable failure, and thus, conforming to the fail-safe concept.

In this context, knowledge of the structure-property relationships at the sub-macroscopic level is one of the key questions that is approached both, experimentally and by modelling. Lifetime performance of long-term operated steel pipelines was investigated based on degraded pipeline materials [2] as well as based on numeric simulations [3]. Thereby, the decrease of the material's resistance against cracking due to degradation mechanisms at nano- and microscopic scale are considered. In service, numerous microstructural features (like inclusions, pores, grain boundaries) as well as technical features due to manufacturing and service loading (like joints, surface roughness or corrosive surface modification) lead to stress concentrations in the component which may result in local plastic deformation and subsequent damage. Ductile failure processes can roughly be divided into plastic deformation, microcavity and microcrack formation, and macroscopic crack growth resulting from cavity and microcrack coalescence [4]. The role of the banded ferrite-pearlite grains during initial cracking has been proven by tracking microstrains with the digital image correlation method by employing the grained structure as speckle pattern [5]. Another chance of experimentally mapping the scenario of crack initiation and accumulation is the Acoustic Emission (AE) technique. AE is capable since it is sensitive to transient elastic waves generated by structural changes such as crack events at microscopic (and macroscopic) scale [6]. Due to its higher sensitivity to microscopic events [7], the AE monitoring of HSLA steels' (High Strength Low-Alloyed) elastoplastic fracture behaviour, which was investigated using compact tension specimens, revealed the crack initiation significantly earlier compared to crack length measuring techniques. Nevertheless, an accurate detection of crack initiation is essential for understanding the material's elastoplastic fracture mechanics. Until

* Corresponding author.
E-mail addresses: Franziska.Baensch@bam.de (F. Baensch), Wolfram.Baer@bam.de (W. Baer), Peter.Wossidlo@bam.de (P. Wossidlo), Karim.Habib@bam.de (A.K. Habib).

https://doi.org/10.1016/j.ijpvp.2022.104863
Received 15 December 2021; Received in revised form 19 November 2022; Accepted 24 November 2022
Available online 25 November 2022

today, the detection and localization of crack initiation are key challenges in structure monitoring and place a high demand on the acquisition setup. Former studies focused on that question employing AE monitoring compared to direct current potential drop (DCPD) and other methods such as ultrasonic measurements (US) demonstrate reasonable agreement of the different methods [[8,9]].

Generally, the AE sensitivity performance is strongly depending on the background noise during a test. To enhance the reliability of detection of low amplitude AE in a noisy environment, other approaches are required than the signal crossing of a (related to background noise) predefined threshold [10–12]. For a quantitative AE analysis of the physical mechanisms of crack formation and growth, a conventional analysis of the AE time signals is rather insufficient [13]. Since material degradation processes are of discrete short duration, they are broad band in frequency domain with frequencies up to 1 MHz or even higher. Thus, AE source identification requires analysis of frequency spectra, whereby the weighted peak frequency (WPF) is found to be the most characteristic feature of a spectrum combining peak frequency and center of gravity in a single figure [14]. In case of brittle cracks, large and rapid changes in stress generate high amplitude elastic waves and broad band spectra. On contrary, in case of ductile cracking with testing of rather tough steels, AE is limited since most of the energy is spent to enlarge the plastic zone. By this, the tip of the crack is blunted and only less energy drives the elastic wave propagation. Consequently, AE events of low peak amplitudes and low frequent spectra are generated [15].

For the present study an experimental setup was further developed which had originally been designed at BAM in the 1990's to study deformation and failure behaviour including crack initiation and growth on large steel pipes by means of DCPD, Ultrasonic (US) and AE methods [8]. It is worth noting that the DCPD behavior recorded in a pipe bending test is much different from common schematic DCPD plots with fracture mechanics tests, where frequently ideally linear graphs up to crack initiation are supposed. Therefore, a new method for the analysis of DCPD data has been established in this study.

The detection of crack initiation at microscopic scale and correlation with distinct source mechanisms remains a challenge and requires at least a close positioning of the AE sensors to the predefined weak point [13]. This approach enables valid AE analyses based on located crack growth and failure events also of broad band character. In contrast to earlier investigations [8,9], the AE monitoring in the present study was carried out continuously in non-threshold mode and data were post processed to identify the point of crack initiation and localization.

2. Experimental approach and data processing

2.1. Test setup

A four-point bending test (Fig. 1) was carried out on a pipe segment made of steel grade S355J2H, which is rather a low carbon structural steel. The tested pipe segment of 2.5 m length has a wall thickness of 16 mm and an outer diameter of 168 mm. Centered at 1.25 m length, a 90 °outer circumferential notch was shaped into the pipe wall by a CNC machine (Fig. 2). The notch has an opening angle of 90°, a notch root radius of 0.2 mm and a ratio of wall thicknesses of 0.5. The bending test was performed using a 4 MN universal testing machine operating hydraulically. The test was driven position controlled with a test speed of 0.25 mm min^{-1}. The pipe was loaded monotonically interrupted by two partial unloadings to adjust measurement equipment. For synchronization, the load (F) and deflection (f) signals were fed into the DPCD and the AE acquisition.

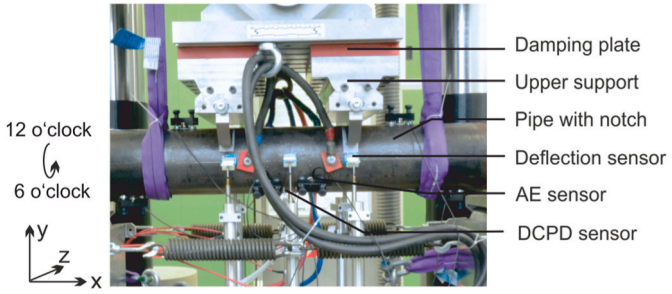

Fig. 1. Experimental setup for a four-point bending test at a 2.5 m long pipe segment using six deflection sensors, five DCPD sensors and four AE sensors to monitor the pipes deformation, damage, and failure behavior.

For deflection measurement, six angles were glued to the pipe at the 3 o'clock and 9 o'clock positions as technical aid for the deflection sensors (Fig. 2(a)). For the DCPD measurement, a DC of 300 A was injected and the potential drop U (or Pot) was measured at five positions close to the notch (Fig. 2(a)), whereby the positions of potential 1–3 are focused further on here (Fig. 3).

Moreover, the test was monitored by non-threshold acoustic emission (AE) measurement using a digital AE equipment AMSY-6 in continuous mode with a sampling rate of 3.33 MHz. To ensure the detection of crack events, four broadband sensors of type VS900-M with a sensitivity between 100 kHz and 900 kHz were arranged in a square around the notch with approximately 50 mm distance to the notch (Fig. 2(a)). The response of the sensors is characterized by resonances at 190 kHz and 350 kHz accompanied by anti-resonances at 200 kHz and 400 kHz (Fig. 4). Above 400 kHz the sensors show a flat response. The AE sensors were fixed with magnetic holders. Coupling agent was a reusable adhesive (Bostik Prestik). To enable good coupling of all sensors, the corrosion layers were removed by grinding surface at the appropriate areas along the pipe. For noise reduction during testing, Teflon sheets were inserted in between the contact area of the pipe wall and the load bearings. Furthermore, PVC damping plates were assembled into the bearing elements (Fig. 1). By this, the acoustic noise was reduced by approximately −10 dB. Furthermore, the test object's near field behavior of up to 15 dB attenuation within the first 32 cm propagation path between source and sensor must be taken into account.

2.2. DPCD data processing

It is worth noting that the DCPD behavior recorded in the pipe bending test is much different from common schematic DCPD plots in fracture mechanics test standards such as ISO 12135 [16] or ASTM E 1820 [17], where the graph is ideally linear up to crack initiation as shown in Fig. 5. Therefore, a new method for the post-test analysis of the DCPD data has been established in this study and is schematically presented in Fig. 6.

Basically, the deformation and failure behavior of the pipe during plastic deformation can be described by blunting of the notch, plastic constriction of the notched section, increase of dislocation density in the crystal lattice and ductile damage processes such as void formation and coalescence as well as microcrack formation. Additionally, there is an increase in temperature due to plastic deformation and electric current. These different effects superpose upon another. With the pipe, their distinctive quantitative impact on the DCPD is not known in detail or cannot be measured at reasonable effort. However, the sum effect can be measured as increase in DCPD at the notch.

The first derivative of the mathematical approximation function of a measured variable provides information about its slope. Based on that, the potential data U had been normalized by the initial value U_0, fitted by a 5th order polynomial function to get the DCPD-deflection function $U/U_0 = f(f)$ and then differentiated to get deeper insight about characteristic parts of the DCPD curve and distinct changes.

During the plastic deformation of the pipe, two parts, I and II, can be distinguished in the course of the first derivative of the potential-deflection curve (Fig. 6). At the beginning of the plastic deformation, the first derivative curve increases linearly to a large extent for a longer

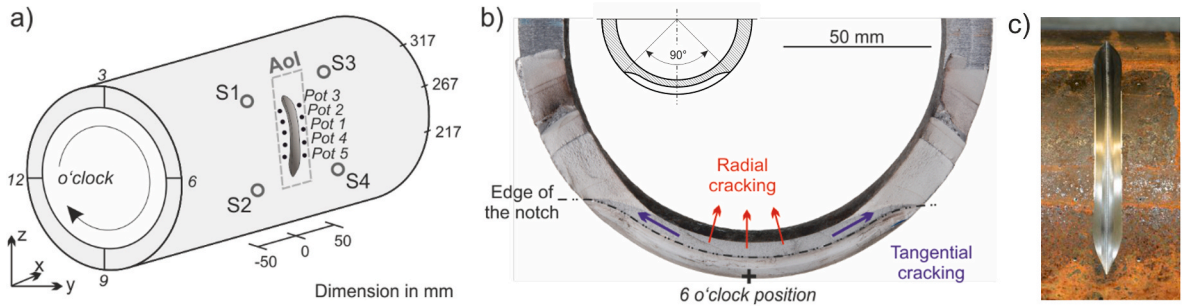

Fig. 2. (a) Coordinate systems (o'clock and mm circumference) on the pipe segment and location of the sensors for the DCPD measurement (Pot 1–5) and for the Acoustic Emission measurement (S1-4). (b) Crack growth in the flawed pipe section emanating from the mechanical notch at the 6 o'clock position. (c) Image of milled 90° mechanical notch having a depth of half of the wall thickness.

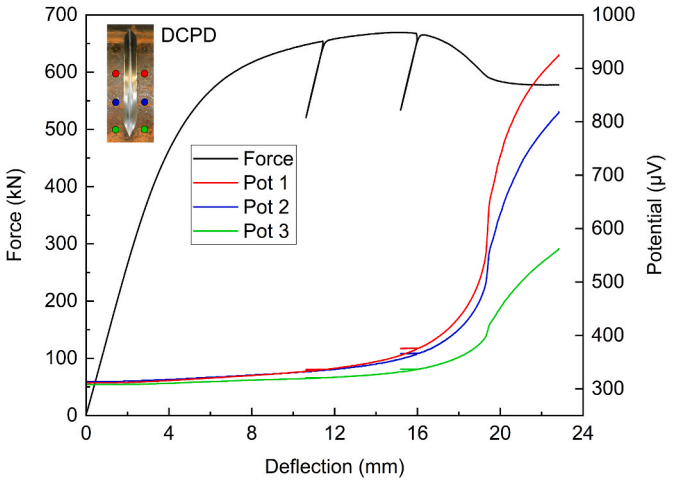

Fig. 3. Force-deflection curves and DCPD during the bending test covering elastic-plastic deformation, crack growth and leakage.

range of deflection, (part I in Fig. 6). Subsequently, the first derivative grows in a significantly progressive manner (part II in Fig. 6). Part I can be associated with a stationary increase of the potential which is caused by the abovementioned deformation and damage effects in the pipe. A significant change in this process will not occur until the process of stable macroscopic crack growth into the pipes wall thickness direction starts (crack initiation) thus commencing part II. From the DCPD point of view, stable crack growth is the only, but governing damage mechanism which additionally comes along the abovementioned plastic deformation and damage effects in the microstructure at this point. Thus, the magnification in DCPD increase during part II can be explained. Depending on the specific data of a test, identifying an exact transition point between parts I and II may be challenging and requires experienced engineering assessment. An uncertainty of approximately ±5% in terms of deflection can roughly be estimated for the initiation value. Due to the small slope of the derivative curve in that region, the uncertainty in terms of force will be smaller than with deflection.

2.3. AE data processing

Applying a high pass filter at 120 kHz is the first step in processing the AE data. By this, the noise from the hydraulical testing device is

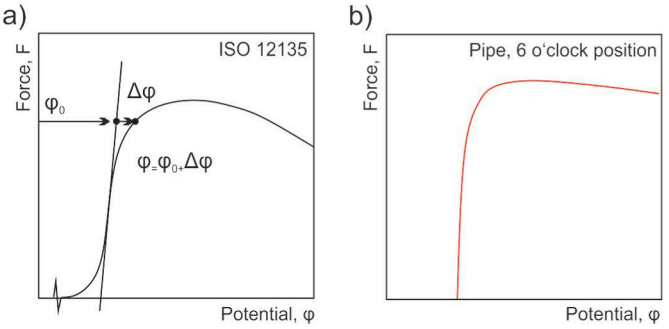

Fig. 5. Schematic potential curves according to ISO 12135 (a) and in case of the pipe bending test (b).

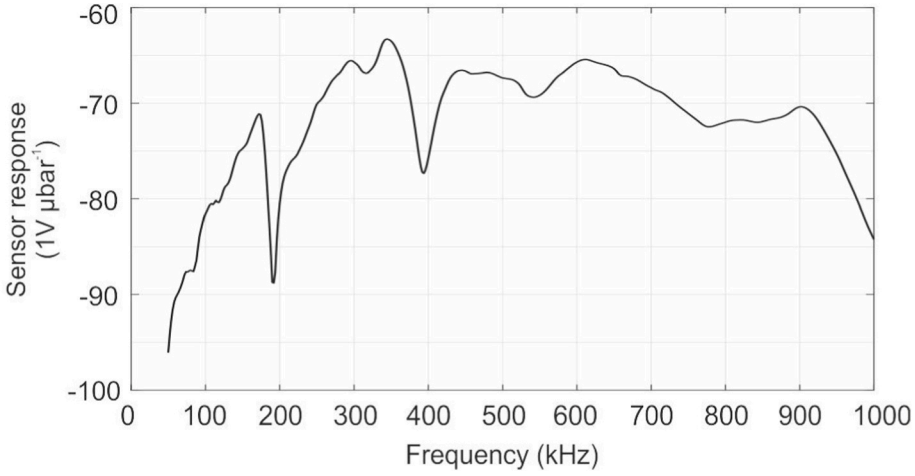

Fig. 4. Averaged frequency response of the four AE sensors VS-900 M.

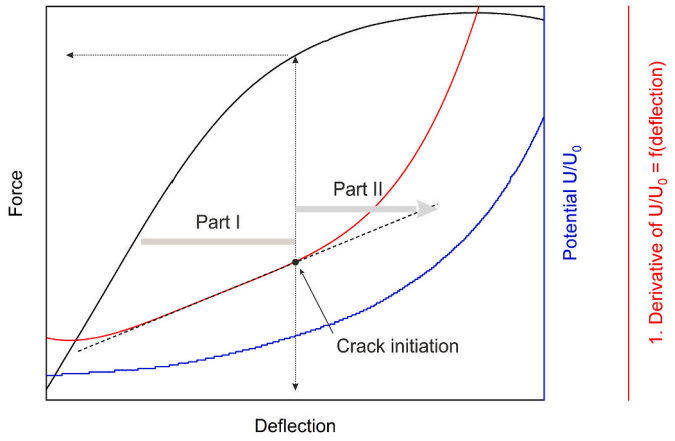

Fig. 6. Schematic on the analysis of DCPD data during deformation, damage and failure of the pipe to determine crack initiation.

eliminated. For AE hit detection, the moving standard deviation σ^2 of the voltage amplitude values A is calculated within a moving window size of 513 samples with the sample of observation centered, compare equation (1). Furthermore, to level low deviations in A relative to higher ones, the logarithm of the moving standard deviation $\log \sigma^2_{i,max}$ is employed. The AE noise level during the test is evaluated by the root mean square (RMS) of detected AE amplitudes represented for an integration time of about 0.0768 ms (256 samples, 3.33 MHz sampling rate). Since the noise level changes with progressing test (Fig. 7), detecting AE hits by means of a moving threshold was proven suitable, as shown in Fig. 8. Therefore, the empirical threshold value of log 2.8 is added to the maxima of $\log \sigma^2_{i,max}$ within the 577 samples before the sample of observation, see Eq. (2). The threshold crossing is defined as the time of arrival (TOA) at the sensor (Fig. 8(c)). Only AE events detected by all four sensors (located events, LEV) are evaluated for further analysis. Based on difference in TOA at the sensors, the AE events are localized in 2D at the pipe surface (Fig. 9(a)). The localization algorithm is based on the determined in-plane AE wave propagation velocity of 4695 ms^{-1}. As soon as the leakage was reached, the localization of AE between all four sensors became worse (Fig. 10). Spectral analysis is applied to the filtered signals detected by the first hit sensor cut from the threshold crossing to a path length of 512 samples. For fast Fourier transformation, all signals are normalized to a peak amplitude of 1 and multiplied by the hamming window. The weighted peak frequency *WPF* is defined in Eq. (3) and was calculated from the spectra limited between 120 kHz and 900 kHz. An overview of the setting parameters for AE monitring and analysis is given in Table 1.

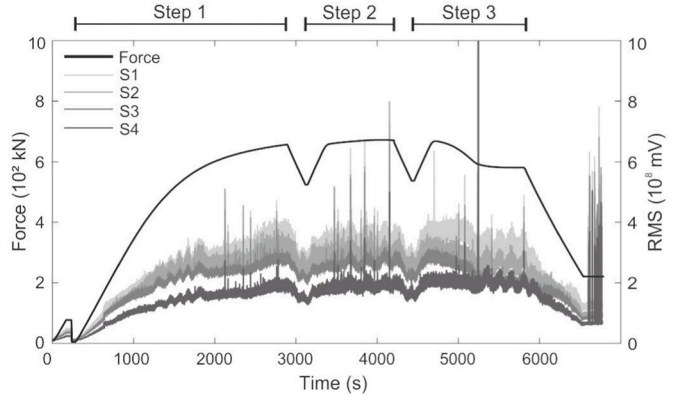

Fig. 7. Loading curve of the bending test and root means square (RMS) of Acoustic Emission with an integration time of 0.0768 ms (256 samples, 3.33 MHz sampling rate) detected by the sensors S1-4.

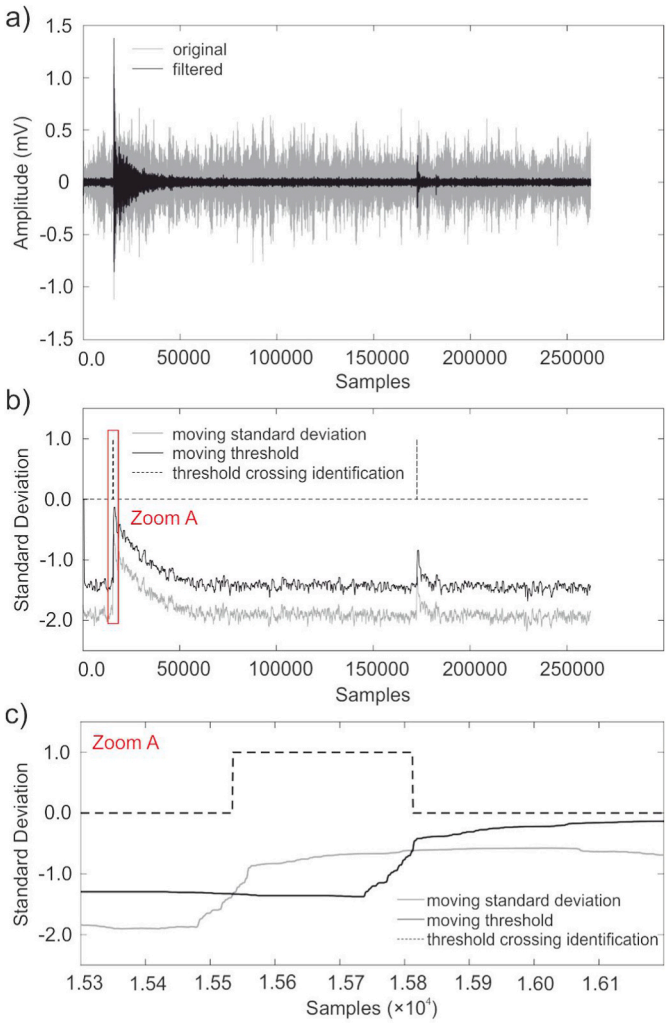

Fig. 8. Acoustic Emission (AE) hit detection in continuously monitored data. (a) Original and filtered signal in (mV). (b) Crossing (dashed line) of the moving threshold (black line) with the moving standard deviation (grey line). (c) Zoom in A showing the AE hit detection in continuously monitored data. Time of arrival estimation based on the moving threshold (black line) crosses (dashed line) the logarithm of the moving standard deviation (grey line).

$$\sigma^2 = \frac{1}{N-1}\left[\sum_{i=0}^{N-1} A_i^2 - \frac{1}{N}\left(\sum_{i=0}^{N-1} A_i\right)^2\right] \quad (1)$$

N = 513 samples: 256 samples before and 256 samples after the one sample of observation.

A … Voltage amplitude in mV

$$THR = \log_{10}\sigma^2_{i,max} + \log_{10} 2.8 \quad (2)$$

$$WPF = \sqrt{f_{peak} \bullet f_{centroid}} \quad (3)$$

3. Results and discussion

3.1. Macroscopic deformation and failure behavior

The four-point bending test was carried out in position control mode performing three quasi static loading steps (Fig. 10). Loading step 1 was stopped at 654 kN, which is about 98% of 669 kN maximum force yielded at the end of loading step 2. Both loading steps, 2 and 3, started at 534 kN, which is approximately 80% of the force maximum. During loading step 3, the force yielded 99% of prior the force maximum and

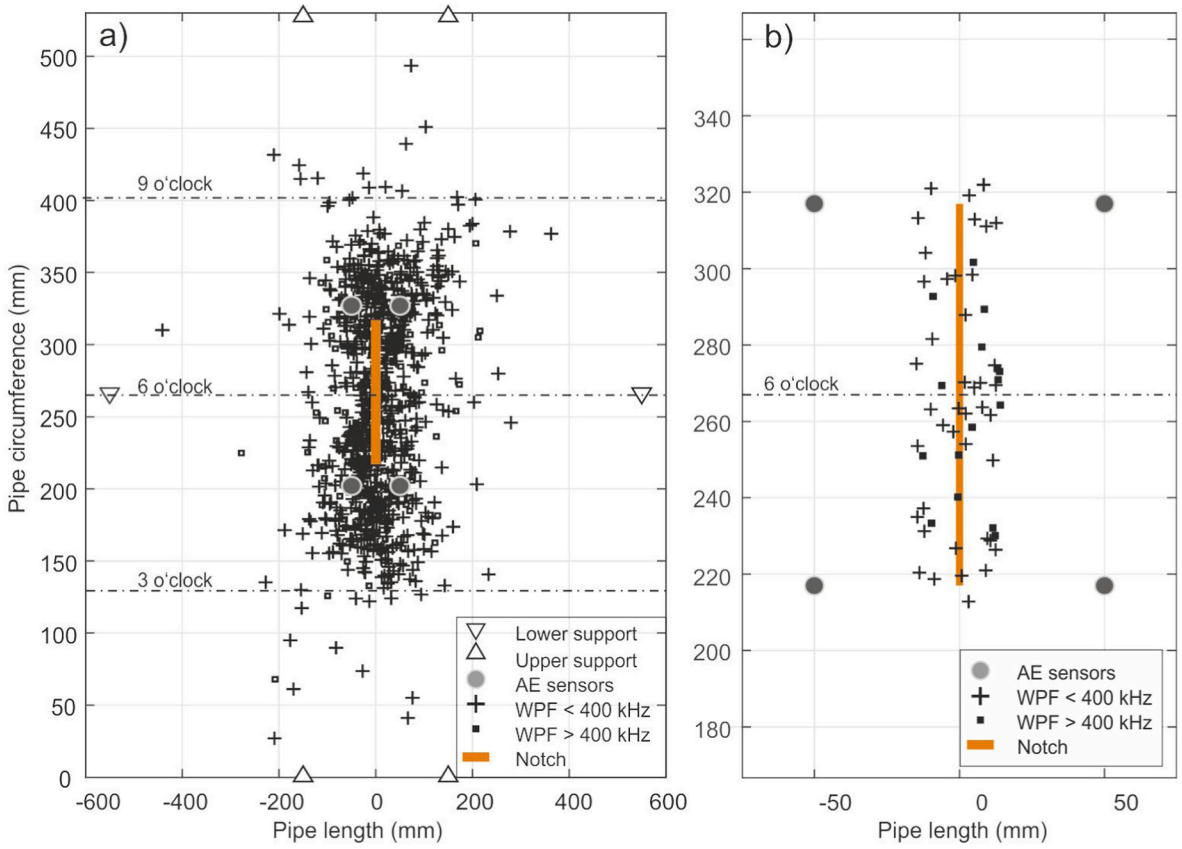

Fig. 9. Acoustic Emission events (LEV) located at a) the whole pipe surface and b) within the area of interest differentiated by signals with weighted peak frequency (WPF).

subsequently decreased while the deflection was further increased. By this behavior the pipe wall breakthrough was signalized. All in all, the deformation and fracture behavior of the pipe segment showed four stages:

(1) Deflection of the pipe and ovalizing of the pipe cross-section were caused by elastic deformation. (Loading step 1)
(2) The onset of plastic deformation was followed by crack initiation and stable crack growth initially in radial direction (Fig. 2(b)). Accompanying processes were the initial blunting of the notch and constriction of the ligament, an increase in the dislocation density and formation and coalescence of voids and microcracks in the metallic microstructure. (Loading steps 1–2)
(3) Overcoming its maximum, the force decreased while the crack finally reached the leakage state (wall breakthrough). (Loading step 3)
(4) With further increase of the deflection of the pipe, the leak opened in a stable manner, and the crack continued to grow at both crack tips (in the direction towards the 3 o'clock and 9 o'clock positions) in the circumferential direction of the pipe wall (Fig. 2 (b)). At this stage the force signal stagnated due to the balance of hardening and crack growth. (Loading step 3)

3.2. Using DCPD for quantitative characterization of microscopic failure behavior

At the beginning of the bend test, the pipe undergoes elastic deformation and ovalization. The DCPD signals remain nearly constant during this period (Fig. 6) since the cross section, the defect structure of the material and the temperature do not change notably. There may even be a small decrease of the potential due to settling effects at the DCPD measurement spots and those spots, where the current is injected. These effects are due to a decreasing electrical contact resistance at the contact points and can be neglected. Subsequently, the pipe deforms plastically and the potential increases progressively. At first, this increase is comparatively moderate until about maximum force. After that, the behavior changes significantly, and the increase of the potential becomes significantly pronounced. Facing that the plot of the potential (Fig. 6) is throughout continuously rising and not showing any distinctive points of change illustrates that a quantitative definition of material damage and failure stages will require more information and further data processing as demonstrated in chapter 2.2. By means of post analyzing the DCPD data, the crack initiation and onset of stable crack growth were determined at 620 kN, 93% of maximum force, corresponding to 8.2 mm deflection. Taking the results of three additional pipe bending tests of the test series into account [18], where crack initiation was detected at force ratios of 0.88, 0.91 and 0.92% of F_{max}, a mean DCPD crack initiation level of 0.91% F_{max} can be ascertained with the material and test setup of the current paper.

3.3. Using AE for quantitative characterization of microscopic failure behavior

After post-processing the continuous data, the onset and localization of AE burst signals, typically generated by structural changes such as crack events, revealed the onset of initial cracks at 527 kN (79% of F_{max}), and thus earlier, i.e. at lower loading levels, than by means of the DPCD method. One must take into consideration that the detection sensitivity to small AE is also affected by far field attenuation between AE event location and AE sensor. A comparison to earlier studies [9] shows that an increase in distance between sensor and notch has a negative impact on the sensitivity to small, initial crack events.

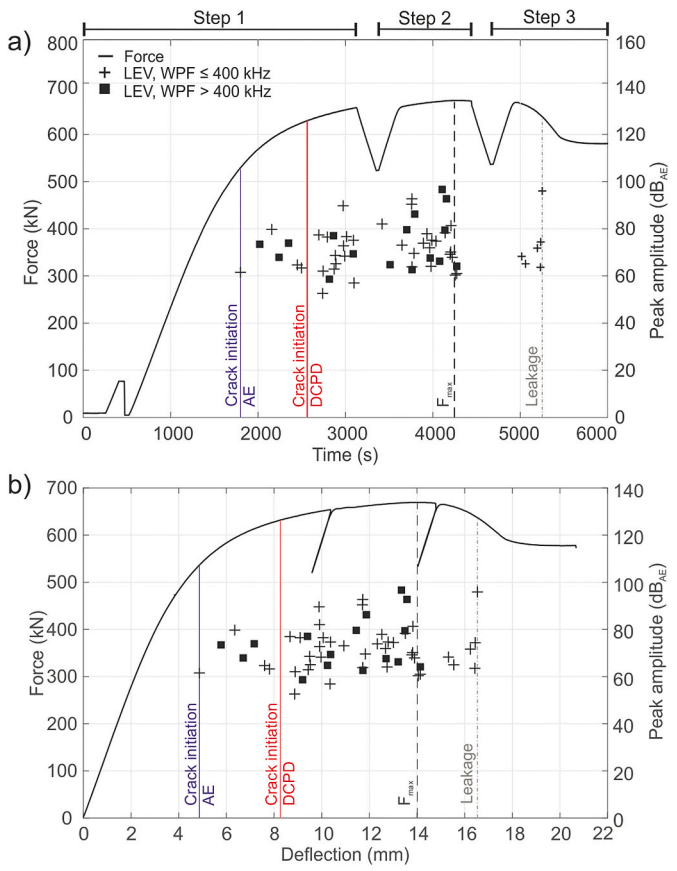

Fig. 10. Applied load corrected peak amplitude and cumulative amplitude of located Acoustic Emission events (LEV) (black) differentiated by their weighted peak frequency (WPF) plotted versus time (a) and deflection (b).

Table 1
Parameters of signal acquisition, location procedure and FFT calculation.

Test and analysis	Parameter
Test duration	appr. 6000 s
Sampling rate	3.33 MHz
Digital filtering	120–1000 kHz
Location procedure	isotropic acoustic propagation
	4695 m s^{-1} acoustic velocity all four sensors detect the AE hit
	AE events of interest are located between ±15 mm close to the notch along pipe length and between 212 mm and 322 mm along the pipe circumference
Fast fourier transformation	Range of interest: 120 kHz–900 kHz
	Filtered signal cut to 512 samples starting at time of arrival (TOA)
	Normalization of the cut signal based on its peak amplitude
	Application of the Hamming window

In total, 877 AE events were located (located event, LEV) over the whole surface of the pipe segment under test (Fig. 9 (a)) prior to leakage. 58 out of those 877 LEV occurred close to the notch within the area of interest (Fig. 9(b)). During the first loading (Fig. 10, step 1), the plastic deformation and accumulation of radial cracks at micro scale had already caused notable damage at the notch. When reloaded in step 2, significant AE appeared at a load level below the previously applied maximum load. Furthermore, the unique maximum value of 97 dB$_{AE}$ of all detected peak amplitudes was detected when the maximum force was reached in load step 2 (Fig. 10). Taking into account the peak amplitude of AE events correlating with the generated defect size, this large AE event reveals a significant damage formation. During loading step 3, no AE occurred during load increase, but AE set on when load decreased with simultaneously increasing deflection. During this state, the second maximum value of 96 dB$_{AE}$ of all detected peak amplitudes occurred. This LEV with high peak amplitude has accompanied the leak opening process at the notch, which started approximately at 5252 s of test duration (see Table 1).

To push the AE analysis forward to more details, the detected LEV need to be linked to their source mechanism what is still a key challenge in AE analysis. A first indication is provided by the signal's intensity, e.g. in terms of energy or peak amplitude, because the AE intensity is in correlation with the size of the generating crack event [19]. Additionally, the frequency spectra of the signals bear the signature of the origin source mechanisms. Therefore, the most characteristic feature to distinguish AE signal's source mechanism is the weighted peak frequency (WPF) since it considers the peak frequency in relation to the spectrum's center of gravity (Eq. (3)). By plotting the signals' peak amplitudes versus the WPF, all 877 LEV measured over the whole test, as well as the 58 LEV detected in the area of interest are found to vary in peak amplitudes between 50 dB$_{AE}$ up to 100 dB$_{AE}$ as well as in a broad range of frequency with WPF between 150 kHz and 600 kHz (Fig. 11 grey and black dots). Caused by the deeply damaged structure (leak open) and, thus, increased acoustic attenuation, the 25 EV from leakage formation reveal the same range in WPF but in a smaller range of peak amplitudes (60 dB$_{AE}$ and 85 dB$_{AE}$) (Fig. 11). Overall, the distribution in peak amplitudes and WPF is rather randomly. For better understanding, artificial cracks simulated by pencil lead breaks (PLB) [20] being executed at the notch in plane and out of plane were evaluated too. Out of plane PLB stimulate transversal waves reflected in a narrow frequency band, which are alike AE of mesoscopic and macroscopic crack growth. In contrast, micro-crack events due to their comparably short duration generate broader banded AE. In plane as well as out of plane PLB, with a lead of 0.5 mm thickness, yielded WPF between 200 kHz and 350 kHz (Fig. 11). These relatively large acoustic events are accompanied by low frequent periodical vibration within the material that addresses both resonance frequencies of the sensor type at 190 kHz and 350 kHz (Fig. 4). Mesoscopic and macroscopic crack events like leak opening are suspected to cause similar effects of wave propagation in the material

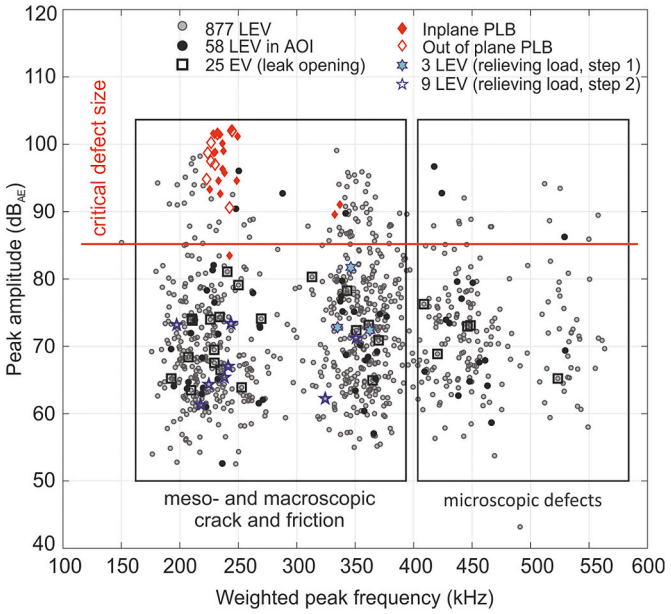

Fig. 11. Signal characterization based on the time signal's peak amplitude versus the weighted peak frequency (WPF) for all located Acoustic Emission events (LEV) under load increase (black and grey) and when relieving load (blue) and for pencil lead breaks (PBL) executed at the notch in and out of plane (red). (For interpretation of the references to colour in this figure legend, the reader is referred to the Web version of this article.)

structure resulting in WPF <400 kHz. The PLB, a crack of half millimeter dimension, generated AE with significant peak amplitudes mainly larger than 85 dB_{AE} (Fig. 11), leading to the assumption that LEV with peak amplitudes above 85 dB_{AE} indicate critical defects. Shortly before leak opened, one LEV of 96 dB_{AE} was detected revealing a relatively high content of low frequencies (Fig. 12). Furthermore, during step 3, while leak opened further, only WPF <400 kHz was detected (Table 2). Comparing the single LEV of 96 dBAe (Fig. 12) with the average of LEV <400 kHz (Fig. 13), the peaks close to 190 kHz and close to 350 kHz are much more pronounced relatively to the high frequency components. Moreover, AE of WPF <400 kHz was also detected immediately when relieving the force after load steps 1 and 2 (see Fig. 11, blue stars). At that time, the AE sources are mutual contact and friction at the crack surfaces when re-closing the crack. Concluding, sources of signals with WPF <400 kHz (Fig. 12) are assumed to be forming mesoscopic and macroscopic defects or friction processes. Besides, the spectra of the single LEV that accompanied the maximum load before macroscopic cracking yielded a peak amplitude of 97 dB_{AE} and WPF >400 kHz (compare black lines in Fig. 12). During the loading steps 1 and 2, approximately 30% of the LEV revealed WPF >400 kHz, whereby, during load step 3, no LEV with WPF >400 kHz was detected (Table 2). Regarding the averaged spectra for WPF >400 kHz, the intensity of high frequency components clearly prevail especially in the range of 400 kHz–600 kHz. In contrast, for the single LEV detected just before maximum load, there is a decrease in spectral intensity above 400 kHz (Fig. 12). However, due to the high frequency content, LEV with WPF >400 kHz are assumed to be generated by microscopic cracks which exhibit a broad band character and are small enough not effecting periodical relaxation processes in the structure.

4. Conclusions

A pre-notched 2.5 m long steel pipe segment was subjected to a four-point bending test in three loading steps in order to quantitatively analyze the crack initiation and growth behavior by means of the AE method. Additionally, crack initiation was investigated by the DCPD method. To enable the detection of small AE events under test conditions with relatively large background noise, the AE measurement was performed non-threshold based and data have been post-processed for the analysis.

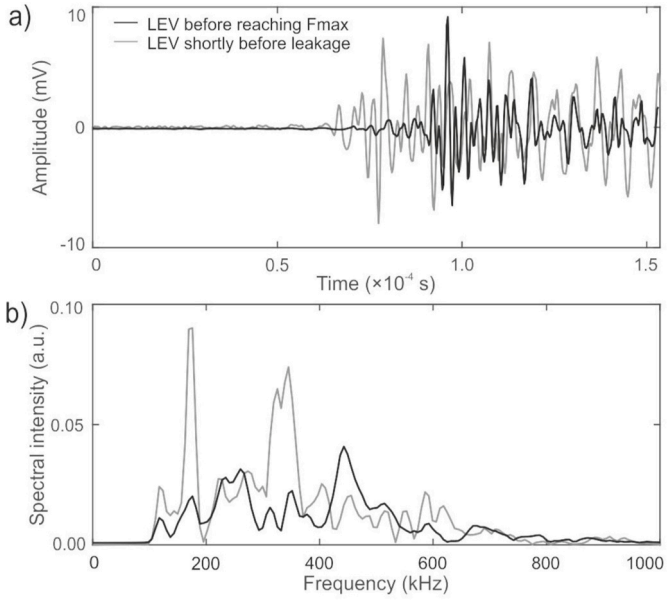

Fig. 12. Comparison of the single LEV detected when yielding maximum load with weighted peak frequency (WPF) < 400 kHz and the single LEV detected shortly before leakage characterized by WPF >400 kHz presented in (a) time and (b) frequency domain.

Table 2
Differentiation of the 58 located AE events (LEV) within the area of interest at the three loading steps by their Weighted Peak Frequency (WPF).

	WPF <400 kHz	WPF >400 kHz
Loading Step 1	17	6
Loading Step 2	19	10
Loading Step 3	6	0

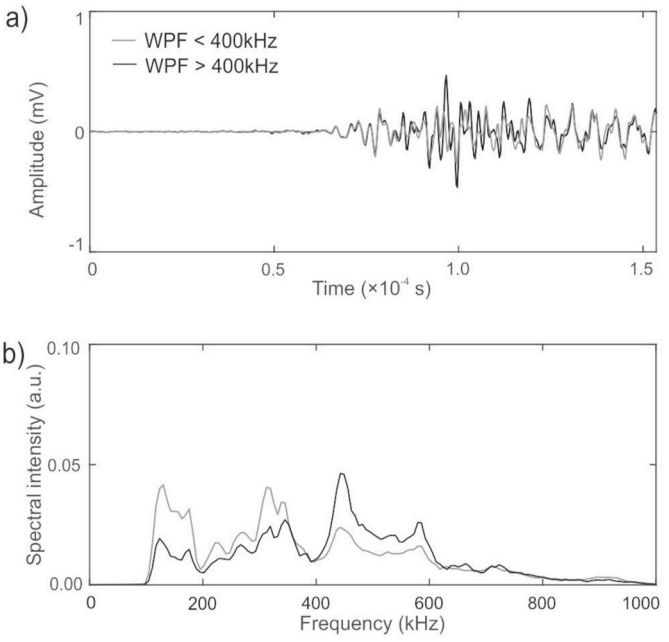

Fig. 13. Average of all located Acoustic Emission events (LEV) with weighted peak frequency (WPF) < 400 kHz and >400 kHz presented in (a) time and (b) frequency domain.

Obtaining quantitative information about crack initiation by means of DCPD technique required post processing of the data measured in the component tests. A new method for DCPD data analysis was established which is based on the consideration of different contributions to material damage as well as features related to the loading. On-site DCPD analysis as supposed with standard fracture mechanics tests does not seem to be feasible in more complex component tests.

Crack initiation was detected earlier by means of AE (79% of the maximum force) than with the DCPD method (92% of the maximum force). To get deeper insight into the sources of the detected AE signals, the weighted peak frequency WPF was analyzed, besides the peak amplitudes (Fig. 11). LEV with WPF <400 kHz are generated by mesoscopic and macroscopic crack events which lead to periodical elastic relaxation waves running through the material and strongly effecting a relatively low frequency spectrum (Fig. 11). Moreover, during reattaining 80% of the previous maximum load after each loading step, slippage and friction from crack closure processes (Fig. 11, blue stars) generate LEV with peak amplitudes below 85 dB_{AE} and WPF <400 kHz. LEV with WPF >400 kHz are implicated to be generated by microscopic crack events.

By this experimental study, the AE measurement was shown to be very suitable for detection of initial crack accumulation at microscopic scale in the frame of fundamental research, but not applicable to real monitoring tasks, yet. All in all, critical mechanisms accompanying the maximum load level and the leak opening were identified by peak amplitudes significantly above 85 dB_{AE}. Herein, the sensors were positioned within the near field to facilitate detection of the acoustic nature of microscopic crack events, while to monitor pipelines, the AE sensors

act within the far field. Moreover, pipeline material, position and number of flanches or welds are affecting the acoustic attenuation, but also e.g. environmental noise due to the location of the pipeline above or below the ground and the type of transported medium (gaseous or liquid) might also affect the detectability. However, the yielded data basis on micro crack events in a steel pipe segment enables the identification of signal features to design sensors adequate for the application, but also to screen for advanced strategies of detection and alarm systems.

As pipelines transport goods like water, gas or oil, which are goods that become more and more very valuable, this infrastructure is becoming an additional importance nowadays. Additionally, due to lacking capacities and resources, pipelines are in operation beyond their operational life [21]. Consequently, the requirements for pipeline monitoring setups are becoming increasingly extensive, demanding 24 h/7 d online setups as well as automated inspections instantly upon need. Therefore, 1) an adequate and robust sensor network for long-term operation must be applied, which combines 2) passive acoustic online monitoring, as required periodically or permanently acting, with 3) transducers allowing active acoustic inspections just in time. Besides AE, the guided wave technique [22,23] as well as the distributed acoustic fiber optic sensing [24,25], find more and more application for pipeline monitoring.

Machine learning algorithms are used for signal processing [26,27] as wells as to classify AE signal types and sources to support the identification of acoustic outliers [14]. Especially in case of critical infrastructure e.g., high pressure gas pipelines, the identification and localization of critical events is of very high priority. In these cases, the analysis time is quite critical and could be reduced by the implementation of artificial intelligence providing decision-making aids in short time [28].

Funding

This research did not receive any specific grant from funding agencies in the public, commercial, or not-for-profit sectors.

Credit author statement

Franziska Baensch: Data Curation, Formal Analysis, Investigation, Methodology, Validation, Visualization, Writing-Original Draft Preparation, **Wolfram Baer:** Data Curation, Formal Analysis, Investigation, Methodology, Validation, Visualization, Writing-Original Draft Preparation, **Peter Wossidlo:** Data Curation, Investigation, Resources, Visualization, **Abdel Karim Habib:** Conceptualization, Methodology, Project Administration, Resources, Supervision, Writing-Review & Editing.

Declaration of competing interest

The authors declare that they have no known competing financial interests or personal relationships that could have appeared to influence the work reported in this paper.

Data availability

Data will be made available on request.

Acknowledgement

This work is part of the project AGIFAMOR within the focus area “Infrastructure” at BAM. The authors would like to thank all partners of the project for fruitful discussions and exchange of ideas.

References

[1] J. Schmidt, N. Schmidt, J. Biernath, Pipeline security – public awareness and mitigation of third party accidents as new layer of protection for the critical infrastructure gas, in: Pipeline Technologiy Conderende 2017, Proc. of PTC, Berlin, Germany, 2017.
[2] P. Maruschak, I. Danyliuk, O. Prentkovskis, R. Bishchak, A. Pylypenko, A. Sorochak, Degradation of the main gas pipeline material and mechanisms of its fracture, in: J Civ Eng Manag, 2014, pp. 864–872, https://doi.org/10.3846/923730.2014.971128, 20(6).
[3] H. Nykyforchyn, O. Zvirko, I. Dzioba, H. Krechkovska, M. Hredil, O. Tsyrulnyk, O. Student, S. Lipiec, R. Pala, Assessment of operational degradation of pipeline steels, in: Materials, 2021, p. 3247, https://doi.org/10.3390/ma14123247, 14(12).
[4] U. Krupp, Mikrostrukturelle Aspekte der Rissinitiierung und -ausbreitung in metallischen Werkstoffen, Postdoctoral thesis, Department of Mechanical Engineering, University Siegen, Germany, 2004.
[5] X. Zhang, Y. Wang, N. Guo, Y. Wang, R. Li, C. Zhang, Y. Zhuuo, Effect of ferrite/pearlite banded structure on the local deformation and crack initiation at notches in pipeline steel, in: Eng Fract Mech, 2020, 107244, https://doi.org/10.1016/j.engfracmech.2020.107244, 237.
[6] C.U. Grosse, M. Ohtsu, D.G. Aggelis, T. Shiotani, Acoustic Emission Testing. Basic for Research – Applications in Engineering, second ed., Springer Nature, Switzerland AG, 2021.
[7] J. Kumar, C.K. Mukhopadhyay, V. Kumar, Monitoring of elastoplastic fracture behavior of HSLA steel using acoustic emission testing, in: Mater Eval, 2021, pp. 383–390, https://doi.org/10.32548/2021.me-04137, 2021, 79(4).
[8] D. Aurich, W. Baer, R. Häcker, D. Klingbeil, K. Ohm, Analyse und Weiterentwicklung bruchmechanischer Versagenskonzepte, Schwerpunkt: Anwendung fortgeschrittener zähbruchmechanischer Konzepte; Bruchübergang. BAM research report 232, Bundesanstalt für Materialforschung und -prüfung, Berlin, 1999.
[9] F. Baensch, W. Baer, P. Wossidlo, A. Habib, Non-threshold acoustic emission analysis of damage evolution in pipe segments of steel S355J2H under bending load, in: 33rd European Conference on Acoustic Emission Testing, Proc. of EWGAE, Senlis, France, 2018.
[10] T. Krietsch, J. Bohse, Selection of acoustic emission and classification of damage mechanisms in fibre composite materials, in: 14th International Acoustic Emission Symposium & 5th Acoustic Emission World Meeting, Proc. of IAES, Big Island Hawai, USA, 1998.
[11] E. Agletdinov, D. Merson, A. Vinogradov, New method of low amplitude signal detection and its application in acoustic emission, in: Appl Sci, 2020, p. 73, https://doi.org/10.3390/app10010073, 10(1).
[12] S.F. Karimian, M. Modarres, H.A. Bruck, A new method for detecting fatigue crack initiation in aluminum alloy using acoustic emission waveform information entropy, in: Eng Frac Mech, 2019, 106771, https://doi.org/10.1016/j.engfracmech.2019.106771, 223.
[13] H.N.G. Wadley, C.B. Scruby, J.H. Speake, Acoustic emission for physical examination of metals, Bar Int. 25 (1) (1980) 41–64, https://doi.org/10.1179/imtr.1980.25.1.41.
[14] M.G.R. Sause, A. Gribov, A.R. Unwin, S. Horn, Pattern recognition approach to identify natural clusters of acoustic emission signals, in: Pattern Recognit Lett, 2012, pp. 17–23, https://doi.org/10.1016/j.patrec.2011.09.018, 33(1).
[15] C.B. Scruby, Quantitative acoustic emission techniques, in: R.S. Sharpe (Ed.), Research Techniques in Nondestructive Testing vol. 8, Academic Press Inc., London, England, 1985, pp. 141–210.
[16] Metallic Materials - Unified Method of Test for the Determination of Quasistatic Fracture Toughness, 2021. ISO 12135.
[17] Standard Test Method for Measurement of Fracture Toughness, ASTM E, 2020, https://doi.org/10.1520/E1820-20B, 1820 20b.
[18] W. Baer, P. Wossidlo, Anwendung der verteilten akustischen und faseroptischen Sensorik zur kontinuierlichen Überwachung von Rohrleitungen, BAM-Test report BAM-9.1/1136, BAM Berlin, Unter den Eichen, Berlin, 2019, 12205, 87.
[19] M.V. Lysak, Development of the theory of acoustic emission by propagating cracks in terms of fracture mechanics, Eng. Fract. Mech. 55 (3) (1996) 443–452, https://doi.org/10.1016/0013-7944(96)00026-4.
[20] M.G.R. Sause, Investigation of pencil-lead breaks as acoustic emission sources, in: J Acoust Emiss, 2011, 29.
[21] B. Koppens, R. Denys, S. Hertelé, A. Lefevre, Pipeline renewal or lifetime extension?, in: Ageing Pipelines Conference Proc., Ostend, Belgium, 2015.
[22] M. Abbas, M. Shafiee, Structural health monitoring (SHM) and determination of surface defects in large metallic structures using ultrasonic guided waves, Sensors 18 (2018) 3958, https://doi.org/10.3390/s1811395.
[23] Z. Wang, S. Huang, S. Wang, S. Zhuang, Q. Wang, W. Zhao, Compressed sensing method for health monitoring of pipelines based on guided wave inspection, in: IEEE Transactions on Instrumentation and Measurement, 2020, pp. 4722–4731, https://doi.org/10.1109/TIM.2019.2951891.
[24] P. Stajanca, S. Chruscicki, T. Homann, S. Seifert, D. Schmidt, A. Habib, Detection of leak-induced pipeline vibrations using fiber-optic distributed acoustic sensing, Sensors 18 (9) (2018) 2841, https://doi.org/10.3390/s18092841.
[25] A.A. Zhirnov, T.V. Choban, K.V. Stepanov, K.I. Koshelev, A.O. Chernutsky, A. B. Pnev, V.E. Karasik, Distributed acoustic sensor using a double sagnac interferometer based on wavelength division multiplexing, Sensors 22 (7) (2022) 2772, https://doi.org/10.3390/s22072772.

[26] van den Ende, M., Lior, I., Ampuero, J.P., Sladen, A., Ferrari, A., & Richard, C. A Self-Supervised Deep Learning Approach for Blind Denoising and Waveform Coherence Enhancement in Distributed Acoustic Sensing Data.
[27] Q. Wu, C.-M. Lee, A modified leakage localization method using multilayer perceptron neural networks in a pressurized gas pipe, Appl. Sci. 9 (9) (2019) 1954, https://doi.org/10.3390/app9091954.
[28] Y. Li, Y. Bao, Review on automated condition assessment of pipelines with machine learning, Adv. Eng. Inf. 53 (2022), https://doi.org/10.1016/j.aei.2022.101687, 101687.